

Critical wetting in the two-dimensional Ising ferromagnet confined between inhomogeneous walls

Marta L. Trobo^{1,2} and Ezequiel V. Albano^{1,3,a}

¹ Instituto de Física de Líquidos y Sistemas Biológicos (IFLYSIB), CCT La Plata. CONICET, UNLP. Calle 59, No. 789, 1900 La Plata, Argentina

² Departamento de Ciencias Básicas, Facultad de Ingeniería, Universidad Nacional de La Plata (UNLP), 1900 La Plata, Argentina

³ Departamento de Física, Facultad de Ciencias Exactas, Universidad Nacional de La Plata (UNLP), 1900 La Plata, Argentina

Received 25 May 2014 / Received in final form 28 October 2014

Published online 15 December 2014 – © EDP Sciences, Società Italiana di Fisica, Springer-Verlag 2014

Abstract. We present a numerical study of the critical wetting behavior of an Ising magnet confined between two walls, separated by a distance L , where short-range inhomogeneous surface magnetic fields act. So, samples are assumed to have a size $L \times M$, L being the width and M the length, respectively. By considering surface fields varying spatially with a given wavelength or period (λ), $H_1(x, \lambda)$ with $1 \leq x \leq M$, we found that the wetting temperature is given by the exact result of Abraham [D.B. Abraham, Phys. Rev. Lett. **44**, 1165 (1980)] provided that an effective field given by the spacial average value ($H_{\text{eff}} \equiv \frac{1}{\lambda} \int_0^\lambda H_1(x, \lambda) dx > 0$) is considered. The above results hold in the low wavelength regime, while for $\lambda \rightarrow \infty$ and a bivaluated surface field (i.e., H_{max} for $x \leq M/2$, and δH_{max} for $x > M/2$, with $0 < \delta < 1$), one observes two almost independent wetting transitions, both being compatible with Abraham's exact results corresponding to H_{max} and δH_{max} , respectively. On the other hand, for $H_1(x, \lambda) \neq 0$ but $H_{\text{eff}} = 0$ bulk standard critical behavior results is observed.

1 Introduction

The study and characterization of the properties of both single component systems and mixtures in confined environments have since long time attracted considerable attention due to their relevance in many practical applications, as well as by the emerging interesting physical challenges. In fact, confined geometries strongly modify the phase behavior of physical systems through a combination of finite-size effects (arising from the finite thickness of the confining container) and surface effects (arising from the interaction of the physical system with the walls), the understanding of these modifications being a topic of relevance in statistical physics, thermodynamics, material science, nanoscience, etc. [1–12]. In particular, critical wetting transitions become significantly modified in confined geometries since, additionally, one has to consider the constraining effect that the external boundaries exert on interfacial fluctuations. Within this context, it is worth mentioning that while huge effort has been devoted to understanding critical wetting transitions in many physical systems (fluids, colloids, polymers, ferromagnets, etc.) confined between homogeneous walls [1–9], the study of the influence of inhomogeneous and rough confining surfaces has received less attention.

Since it is well known that the surface structure can dramatically change wetting properties, the study of wetting in structured surfaces is a topic that deserves extensive research [9]. In fact, recent advances in nano- and microtechnology [10,12] allow for the construction of patterned surfaces, where wetting properties can be varied spatially in a controlled fashion, as well as structured surfaces such that the surface geometry can be controlled but the chemical structure is the same along the surface [9,13,14]. The ability to control wettability is important for a wide range of technological applications, e.g., when precise microfluidic handling is required. In this way, by using predesigned surfaces roughness at a micro- or nanoscale, one can enhance the wetting properties of solid material. In fact, it is known that surface roughness affects wetting properties since the effective contact angle becomes smaller when the roughness increases [15–18]. Also, the combined effects of roughness and heterogeneity can dramatically change the wettability of a surface leading, e.g., to superhydrophobicity [14]. Furthermore, rough surfaces can be created by adding square pillars on a flat surface. In this way, the surface roughness can be altered by varying the pillar width and interpillar spacing [19,20]. In this case by means of molecular simulations, it has been shown that a hydrophilic surface can be converted into a hydrophobic one by changing its roughness [19].

^a e-mail: ezequielalb@yahoo.com.ar

Within this broad context, the aim of this paper is to contribute to understanding the effects caused by surface heterogeneity on the wetting behavior from a basic point of view based on statistical physics and numerical simulations. For this purpose, we consider geometrically uniform (flat) confinement surfaces where their heterogeneity can be modeled by a suitable change of the interaction energy between different components of the surface and the confined system. Also, we will focus our study on the $d = 2$ Ising ferromagnet in the $L \times M$ ($L \ll M$) geometry, where at the confinement walls, separated by a distance L , laterally inhomogeneous (short-range) surface magnetic fields act [21]. In fact, it is well known that the $d = 2$ Ising magnet confined between antisymmetric walls exhibits a localization-delocalization transition of the interface between domains of different orientations, which is the precursor of a true wetting transition occurring in the thermodynamic limit [21–26]. Within this context, let us mention that recently we have proposed a scaling theory for wetting transitions that has been numerically tested for the Blume-Capel model confined between walls where homogeneous magnetic surface fields are applied [24,25]. Therefore, the present paper is an attempt to take advantage of that existing theory in order to generalize its validity to the case of inhomogeneous fields.

Similar geometries (with inhomogeneous surface fields) have previously been employed in order to study the critical Casimir force in thin films and in the Ising universality class [27,28]. In fact, Parisen Toldin et al. [27,28] considered that one of the confining surfaces is homogeneous, while the opposing one is chemically striped, such that there is a laterally alternating adsorption preference, which is implemented by laterally inhomogeneous surface fields alternating in sign. Also, it is worth mentioning that in a recent paper, Fytas and Selke [29] have studied wetting transitions by using the three-state Blume-Capel model. These authors have employed special boundary conditions, modifying the exchange interaction at one of the boundaries by introducing, at one wall, the surface coupling $\alpha \times J$ between the boundary spins and the neighboring bulk spins, with $0 \leq \alpha \leq 1$. Otherwise, the couplings between neighbor spins are always J . Additionally, very recently we studied wetting transitions by considering flat confinement walls, but the magnetic field is taken to be nonuniform by adopting the values $H_1, \delta H_1, H_1, \delta H_1, \dots$ for adjacent sites along the walls [21]. Here $-1 < \delta < 1$ is a parameter that allows us to control the degree of nonuniformity of the surface field. Of course, the case $\delta = 1$ (uniform field) corresponds to the standard case whose phase diagram was worked out exactly by Abraham [30], such that

$$\begin{aligned} H_{1w}(T)/J &\equiv F(T) \\ &= (k_B T/2J) \left\{ \cosh^{-1} \left[\cosh(2J/k_B T) \right. \right. \\ &\quad \left. \left. - \sinh(2J/k_B T) \exp(-2J/k_B T) \right] \right\}, \quad (1) \end{aligned}$$

where H_{1w} is the value of the surface field for the second-order wetting transition that takes place at the corresponding wetting temperature $T \equiv T_w$, and k_B is the Boltzmann constant.

Based on numerical Monte Carlo results and ground state considerations, we conjectured that these inhomogeneous surface wetting transitions may occur at effective fields given by [21]

$$H_{\text{eff}}/J = F(T). \quad (2)$$

We consider a nonuniform field varying along the x direction parallel to the walls but having a spatial wavelength or period $\lambda \leq M$. The effective field H_{eff} at a λ coarse-grained level is given by a simple average, namely,

$$H_{\text{eff}} = \frac{1}{\lambda} \sum_{x=1}^{\lambda} H_1(x, \lambda), \quad (3)$$

and equation (2) holds for $H_{\text{eff}} > 0$, so that the inhomogeneous surface field has essentially a preferential direction and the formation of antiferromagnetic surface structures is avoided. So, in this paper we present a more extensive study of wetting behavior in the case of periodically varying fields of larger wavelength ($2 \leq \lambda \leq 128$). Also, the long wavelength regime, namely, $\lambda \rightarrow \infty$, is studied.

Finally, it is worth discuss and stress the relevance of the present manuscript for the understanding of critical phenomena in confined geometries and in $d = 2$ dimensions, within the broad context of basic studies in the field of statistical mechanics, as well as to discuss possible scenarios for the applications of our findings for the study of adsorption phenomena [31] and magnetism in two-dimensions [32]. In fact, phase transitions in adsorbed monolayers at surfaces [31,32] are both of practical and fundamental interest: the understanding of physical and chemical properties of surfaces with adsorbed layers is a prerequisite for the description of phenomena such as catalysis, corrosion, nucleation and growth upon crystal formation, etc. Then, let us recall that our confined geometry of size $L \times M$ is a suitable model for a terrace of an stepped surface [23], where L is taken as the terrace width, being M its length. Furthermore, the square lattice used in our study represents the (100) surface of a cubic crystal. Then, we assume that the substrate surface provides a strongly corrugated adsorption potential, so that adsorption can be described in terms of the lattice gas model. Now even the surfaces of single crystals are never perfectly flat but contain surface steps, and such steps clearly affect adsorption phenomena [31,32].

While in most cases adsorption takes place preferentially at the steps (e.g. for $i = 1$ or $i = L$ in our sample with $1 \leq i \leq L$), see e.g. [33], recent studies of Xe adsorption at surface steps have indicated differences in the preferred adsorption sites on different metals. On Pt(111), these sites are on the low-coordination top edges of steps [34,35]; whereas on other surfaces such as Cu(110) [36], Ag(111) [37], and Cu(111) [38], these sites are at the high coordination lower edges. On the other hand, in some cases preferential adsorption on terraces has also been reported [39]. Such differences in the interaction of adsorbed species at surface steps can have consequences for the subsequent growth of the films. Within this context, it is worth mentioning that the adsorption

and desorption of Xe on Pt(997), which is a stepped surface having terraces of Pt(111), have been the subject of several experimental studies [40–43]. In these studies it has been demonstrated that, at certain temperatures the adsorption of Xe on Pt(997) occurs row by row, namely the discrete and sequential growth of rows of Xe along the step edges has been reported. Such a row by row growth becomes more disordered when increasing the temperature, by keeping the gas pressure constant [41]. A similar growth mechanism was also observed for Kr on the same surface. These results on the displacement of the interface between Xe (or Kr) occupied and empty surface sites are fully consistent with the interface localization-delocalization transition reported in our study: in fact, in our simulations the early detachment of the interface from the wall is equivalent to a smooth growth of rows of adsorbed species in the direction parallel to the steps, while the onset of disorder when the temperature is increased resembles the delocalization of the interface, which is the precursor of wetting in the thermodynamic limit. On the other hand, high-resolution thermal desorption experiments interpreted by using a lattice gas model [42] allow the determination of the binding energies of three different sites on the terraces, as well as the lateral Xe-Xe interaction within the terrace and along the steps. The result was that the binding energies for the Xe were 264, 398, and 287 meV for adsorption on the terrace, at the top of the step, and at the bottom of the step, respectively. So, our choice of different surface magnetic fields at the walls (in our magnetic terminology) are supported by the fact that these fields are straightforwardly mapped into binding energies at step sites when using the lattice gas framework [23].

The understanding of adsorption on stepped surfaces is also relevant for the characterisation of adsorbed metallic, dielectric, and semiconductor monolayers. In fact, recently Wagner et al. [44] have shown that the structure of NaCl layers formed on Cu(110) strongly depends on the presence of surface steps. Also, it has been shown that the preferential adsorption at steps can be used for the monolithic growth of ultrathin Ge nanowires on Si(001) with exotic physical properties [45]. Furthermore, the growth of Fe nanostripes on a vicinal Cu(111) surface has been investigated on the atomic scale by means of various experimental techniques [46] as well as by performing molecular dynamics and kinetic Monte Carlo simulations [47].

On the other hand, it is widely recognized that ultrathin ferromagnetic films are ideal model systems for statistical mechanics models such as the Ising or Heisenberg model, in particular, for the study of critical phenomena [32]. Within this context Zdyb and Bauer [48] have recently reported a multitechnic study of the adsorption of gold on W(100) stepped surfaces, showing that the observed order disorder transition in the adsorbed Au monolayer can be ascribed to the Ising universality class with critical exponents $\beta = 1/8$ and $\nu = 0.99 \pm 0.007$. The effective dependence of the exponent β on the terrace width can be explained within the framework of the theory of finite size effects, in particular, for Ising model lattices, which predicts a shift of the critical temperature and the

rounding of the order parameter (compare e.g. Fig. 2 of Ref. [48] and Fig. 8 of the present paper). Scaling plots of the experimental results (Fig. 5 of Ref. [48]) are in full agreement with our numerical results (inset of Fig. 8a of the present paper). These results point out that a coarse graining of inhomogeneous wall fields of small wavelength, as proposed in this paper, may play a relevant role in interpretation of adsorption experiments on stepped surfaces where the binding energies at step sites are expected to be largely inhomogeneous. Rounding and shifting of order-disorder transitions due to surface steps have also been reported for the adsorption of Fe on W(110) [32], in agreement with our findings discussed in the context of Figures 8a and 8b.

It is worth mentioning that periodically varying inhomogeneous fields, as used in our simulations, naturally emerge in crystalline alloys and solid compounds, where different chemical species are present along the steps, see e.g. the recent study and analysis of the structure of atomic steps on the MgO(100) stepped surface [49], and the characterization of the electronic properties of the Si(557)-Au stepped surface [50]. Also, inhomogeneous steps can also be obtained by oxydation of stepped surfaces, see e.g. [51]. Furthermore, chemical heterogeneous steps capable to influence adsorption phenomena at the terraces, can also be achieved by using modern techniques developed for the construction of nano and micro structured surfaces [9–14]. Another scenery for the study of the effect of periodically varying fields is the use of periodically magnetized audio tapes and other magnetically based storage devices [52]. In fact, these materials have recently been used as substrates for study the adsorption of living and dead magnetotactic bacteria, as well as magnetic nanoparticles [52].

On the other hand, our results raise interesting theoretical challenges in the field of statistical physics. In fact, very recently it has been shown that the presence, at the confinement walls, of randomly distributed (mobile) nonmagnetic impurities could change the nature of the wetting transition, e.g. from critical to complete wetting [53]. In this way, the naive interpretation suggesting that these nonmagnetic species simply screen out the strength of the surface fields does not hold, namely one can not replace the surface magnetic field by some coarse grained effective field and describe the whole scenery within the context of critical wetting with the aid of equation (1). This result is in contrast with the findings reported in the present paper, where we conjectured that the coarse grained inhomogeneous fields can be used as effective fields extending the validity of Abraham's exact results for wetting with short range interactions. We also expect that transfer matrix calculations could shed light on these intriguing results, since that technique has proved to be useful in order to understand wetting behaviour in stripped geometries (see e.g. [54,55] and references therein), however this task is beyond the scope of the present paper.

The paper is organized as follows: in Section 2, we describe the geometry used to simulate the confined Ising ferromagnet, while Section 3 is devoted to a brief overview

of theoretical considerations. In Section 4, we provide a brief description of the simulation procedure, and our results are presented and discussed in Section 5. Finally, we state our conclusions in Section 6.

2 The Ising model with inhomogeneous confinement walls

We consider the Hamiltonian of the Ising magnet in the $d = 2$ dimensional square lattice in an $L \times M$ geometry, where each lattice site i carries a spin S_i that can take only two values, $S_i = \pm 1$ [21]. Periodic boundary conditions are assumed along the x direction, where the lattice is M rows long, while free boundary conditions are used in the y direction where the lattice is L lines long. Furthermore, short-range nonuniform competitive surface fields $H_1(x)$ and $H_L(x)$ act on the first and last rows, respectively. Thus the Hamiltonian reads

$$\mathcal{H} = -J \sum_{\langle i,j \rangle} S_i S_j - H_1(x) \sum_{i \in \text{row } 1} S_i - H_L(x) \sum_{i \in \text{row } L} S_i, \quad (4)$$

where $J > 0$ is the coupling constant between spins placed at nearest-neighbor sites, and the surface fields $H_1(x)$ and $H_L(x)$ act only on the spins placed in the first ($y = 1$) and last ($y = L$) rows, respectively. Notice that the magnetic fields are measured in units of the coupling constant J . For the study of wetting transitions, or more rigorously localization-delocalization effective transitions occurring in finite samples, it is convenient to adopt the antisymmetric situation $H_1(x) = -H_L(x) < 0$ and then consider the thermodynamic limit ($L \rightarrow \infty, M \rightarrow \infty$).

In the present work we studied in detail the influence of three different surface fields, as follows.

- (i) Nonuniform fields varying spatially with a fixed wavelength (λ), given by

$$H_1(x, \lambda) = H_{\max} \sin^2(2\pi x/\lambda), \quad (5)$$

where H_{\max} is the amplitude of the field and the fields acting at opposite walls are antisymmetric, so their average values are $\langle H_1 \rangle = H_{\max}/2$ and $\langle H_L \rangle = -H_{\max}/2$, respectively. Here one has $H_{\text{eff}} = H_{\max}/2$ (see Eqs. (4) and (5)).

- (ii) As in case (i) but assuming a sinusoidal dependence such that the average values of the fields at the walls vanish, i.e.,

$$H_1(x, \lambda) = H_{\max} \sin(2\pi x/\lambda), \quad (6)$$

with $\langle H_1 \rangle = \langle H_L \rangle = H_{\text{eff}} = 0$.

- (iii) Finally, in order to investigate the long-wavelength behavior we considered a bivaluated field of the form

$$H_1(x, \lambda) = \begin{cases} H_{\max} & \text{for } 1 \leq x \leq \lambda/2, \\ \delta H_{\max} & \text{for } \lambda/2 < x \leq \lambda, \end{cases} \quad (7)$$

with $H_{\text{eff}} = H_{\max}(1 + \delta)/2$, when $0 < \delta \leq 1$.

By using the surface magnetic fields given by equations (5)–(7), actually two phase transitions can be observed: one at the bulk critical temperature (T_{cb}) that is the standard order-disorder critical temperature of the Ising magnet, which is exactly known, namely, $\exp\left(\frac{2J}{k_B T_{cb}}\right) = \sqrt{2} + 1$, $T_{cb} \simeq 2.27J/k_B$ [56]. The other, a wetting transition is expected to occur at $T_w(H_{\text{eff}}) < T_{cb}$, at least for $H_{\text{eff}} > 0$. This wetting transition is of second order throughout the regime $0 < H_{\text{eff}} < J$.

3 Theoretical considerations

Recent developments in a finite-size scaling theory [24,25], which rationalize wetting transitions in systems with short-range interactions between the walls and the confined material as a bulk critical phenomenon with order parameter critical exponent $\beta = 0$, allow for a precise determination of the critical points and therefore, the construction of suitable phase diagrams.

During the simulations, we evaluated the total thermal average absolute magnetization of the film, $\langle |m| \rangle$, the square value of the magnetization $\langle m^2 \rangle$ and the fourth-order cumulant U . The total magnetization of the sample involves the summation over the total number of spins ($N = L \times M$) in the sample, i.e.,

$$m = \frac{1}{N} \sum_{i=1}^N S_i. \quad (8)$$

The thermal expectation $\langle |m| \rangle_T$ for $T < T_{cb}$ will be nonzero for the standard order-disorder transition. In contrast, for wetting transitions the absolute value of total magnetization $\langle |m| \rangle$ undergoes a transition from a nonzero value (corresponding to the presence of a localized interface between domains of opposite magnetization) to zero just when the interface becomes delocalized at the effective wetting transition temperature, which can be obtained from simulation results in finite samples but must be extrapolated to the thermodynamic limit in order to obtain the true critical point.

Based on these considerations, it has been proposed [24,25] that the distribution function $P_{L,M}(m)$ of the total magnetization in a finite geometry scales as [57,58]

$$P_{L,M}(m) = \xi_{\parallel}^{\beta/\nu_{\parallel}} \tilde{P} \left(\frac{L^{\nu_{\parallel}/\nu_{\perp}}}{M}, \frac{M}{\xi_{\parallel}}, m \xi_{\parallel}^{\beta/\nu_{\parallel}} \right), \quad (9)$$

an expression that generalizes the standard scaling law for isotropic systems having linear dimension L in all spatial directions [59] to the case with anisotropic correlation length exponents ν_{\parallel} and ν_{\perp} in the directions parallel and perpendicular to the interface, respectively. Now, the fact that M scales with ν_{\parallel} and L scales with ν_{\perp} can be used to show that the finite-size dependence on either L or M enters in the scaling function through “the generalized aspect ratio” $c \equiv L^{\nu_{\parallel}/\nu_{\perp}}/M$ rather than through

the isotropic case where the “aspect ratio” L/M has to be used. The prefactor $\xi_{\parallel}^{\beta/\nu_{\parallel}}$ in equation (9) ensures that the probability distribution $P_{L,M}(m)$ can be properly normalized. Also, by taking suitable moments of $P_{L,M}(m)$ one can derive the following expressions:

$$\begin{aligned} \langle |m| \rangle &= \int_{-1}^1 dm |m| P_{L,M}(m) \\ &= \xi_{\parallel}^{-\beta/\nu_{\parallel}} \tilde{m} \left(\frac{L^{\nu_{\parallel}/\nu_{\perp}}}{M}, \frac{M}{\xi_{\parallel}} \right), \end{aligned} \quad (10)$$

and

$$\langle m^{2k} \rangle = \xi_{\parallel}^{-2k\beta/\nu_{\parallel}} \tilde{m}^{2k} \left(\frac{L^{\nu_{\parallel}/\nu_{\perp}}}{M}, \frac{M}{\xi_{\parallel}} \right), \quad (11)$$

$k = 1, 2, \dots$, where \tilde{m} and \tilde{m}^{2k} are scaling functions that do not need to be specified here. By using (10) and (11) we can obtain the Binder cumulant (U) given by

$$U(T) = 1 - \frac{\langle m^4 \rangle}{[3\langle m^2 \rangle^2]}, \quad (12)$$

which in turn is a valuable observable in numerical simulations (see also below).

Note that for critical wetting in $d = 2$ dimensions there is a single independent critical exponent given by [3]

$$\nu_{\parallel} = 2. \quad (13)$$

Also, the hyperscaling relationship for interfacial phenomena $\nu_{\parallel} = 2 - \alpha_s$ [3] implies $\alpha_s = 0$ for the critical divergence of the surface specific heat. Furthermore, the correlation lengths describing the fluctuations of the interface scale as

$$\zeta_{\perp}^2 \propto \zeta_{\parallel}, \quad \zeta_{\perp} \sim (T - T_w)^{-\nu_{\perp}}, \quad (14)$$

so that $\nu_{\perp} = 1$ [6,7]. Now, by focusing our attention in equations (9)–(11), it follows that for a full scaling description of critical wetting in $d = 2$ dimension one needs to fix the value of β . In recent papers [24,25] by using scaling arguments, we showed that $\beta = 0$ for critical wetting with short-range forces. From the practical point of view, the key results reviewed in this section, namely, $\beta = 0$, $\nu_{\parallel} = 2$ and $\nu_{\perp} = 1$ for critical wetting with short-range surface fields, imply that plots of the magnetization and all its moments, say observables $O(T, L)$, will exhibit generic scaling relationships of the form

$$O(T, L) = \tilde{O}((T - T_w)L^{1/\nu_{\parallel}}, c), \quad (15)$$

where \tilde{O} is a suitable scaling function, which does not need to be specified here, that depends on L and the generalized aspect ratio $c \equiv L^{\nu_{\parallel}/\nu_{\perp}}/M$ (or equivalently on $M = L^2/c$ and c). In this way, those observables measured for different sample sizes will show a common intersection point provided that the “generalized aspect ratio” $c \equiv L^{\nu_{\parallel}/\nu_{\perp}}/M$ is kept constant. This intersection point allows for precise determinations of wetting transition points.

4 Brief comments on the simulation procedure

Simulations are performed by using lattices of width $L = 12, 18, 24, 36, \text{ and } 48$. Also, in most of the numerical work we chose a particular value of the generalized aspect ratio, namely, $c = L^2/M = 9/8$. Of course, the value of the constant c in principle is arbitrary and the results on the location of $T_w(H_{1w})$ should not depend on this choice. Periodic boundary conditions are applied along the x direction (parallel to the confinement walls of length M), while free boundary conditions are taken at the walls where surface fields act. Monte Carlo simulations were then performed using the standard Metropolis algorithm; see e.g., [60] for a review. Typical runs are performed over 20×10^6 Monte Carlo steps per lattice site (MCS), disregarding the first 5×10^6 MCS to allow the system to reach equilibrium. Note that for systems far below bulk criticality exposed to boundary fields, cluster algorithms do not present any advantages [61].

5 Results and discussions

Let us first analyze the case where $H_{\max}(x) > 0$, so that $H_{\text{eff}} > 0$ too. In particular by choosing $H_1(x)$ as given by equation (5), we found that plots of the absolute magnetization $\langle |m| \rangle$, the second moment of the magnetization $\langle m^2 \rangle$, and the cumulant U versus the temperature exhibit a common intersection point, in agreement with the scaling theory outlined in Section 3 (see also [24,25]), which allows us to locate the wetting critical temperature (see Figs. 1–3). In all cases we choose $H_{\max}/J = 1.0$, so that according to equation (5) one has $H_{\text{eff}} = 1/2$. Furthermore, the plots shown Figures 1–3 (which have been obtained for $\lambda = 4, 16, \text{ and } 32$, respectively) confirm that T_w is independent of λ (within our error bars), i.e., we obtained $T_w = 0.875(15)$, as expected if the conjecture outlined in Section 3 holds. We further analyzed the case $\lambda = 128$ obtaining $T_w = 0.91(3)$, where large error bars are a consequence of the larger samples needed in the simulations and the corresponding smaller statistics of our data.

Furthermore, a more convincing test of the conjecture arises from the fact that the exact result worked out by Abraham (Eq. (1)) yields $T_w(H_{\text{eff}} = 1/2) = 0.8615$, in excellent agreement with our measurements. For the sake of completeness, we also tested the finite-size scaling of $\langle |m| \rangle$, $\langle m^2 \rangle$, and U given by equations (10)–(12), as shown in the insets of Figures 1–3, respectively. In all cases we obtained quite reasonable master curves, independent of λ , by using $T_w = 0.875$ as a single adjustable parameter.

Since a systematic study on the validity of the conjecture in the $\lambda \rightarrow \infty$ limit appears as a formidable computational task, due to the larger lattices needed, we addressed the test by an alternative way: considering a bivaluated surface field given by equation (7). In fact, for that situation one has $\lambda \equiv M$, so that the extrapolation $M \rightarrow \infty$ (with $L = \sqrt{cM}$) gives insight into the dependence of wetting transitions on the long-wavelength variations of the

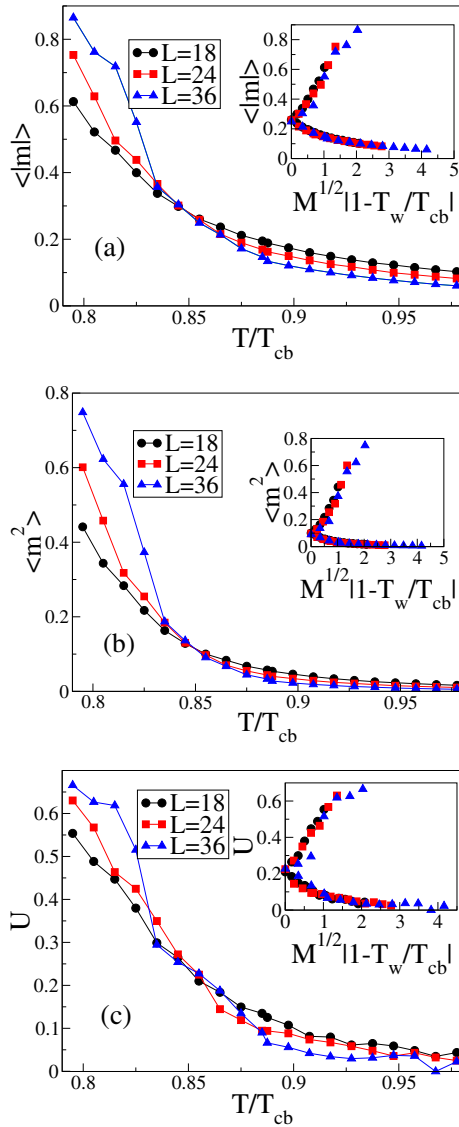


Fig. 1. Plots of (a) the average absolute value of the magnetization ($\langle |m| \rangle$), (b) the average square magnetization ($\langle m^2 \rangle$), and (c) the cumulant (U) versus the temperature relative to the bulk critical point, obtained for samples of different sizes (as indicated). Data corresponding to fields given by equation (5) with $\lambda = 4$ and $H_{\max}/J = 1.00$, so that $H_{\text{eff}} = 0.50$ (see Eq. (3)). All sample sizes have the same generalized aspect ratio $c = L^2/M = 9/8$. The common intersection point at $T_w/T_{cb} = 0.855 \pm 0.01$ allows us to locate the critical wetting temperature [24]. The insets in these figures show the corresponding scaling plots of the observable already shown in the main panel. Further details are given in the text.

surface field, with $H_1(x) > 0$. Figures 4 and 5 show plots of $\langle |m| \rangle$, $\langle m^2 \rangle$, and U versus T obtained for $x = \lambda/4$ and $x = 3\lambda/4$ ¹, respectively. Since we take $H_{\max} = 0.7227$, Figure 4 yields a wetting critical point $T_w = 0.699$, in full agreement with $T_w(H_{\max} = 0.7227) = 0.702843$, that

¹ In order to obtain reliable statistics, the observables are averaged within the range $x - L \leq x^* \leq x + L$, with $x^* = \lambda/4$ and $x^* = 3\lambda/4$.

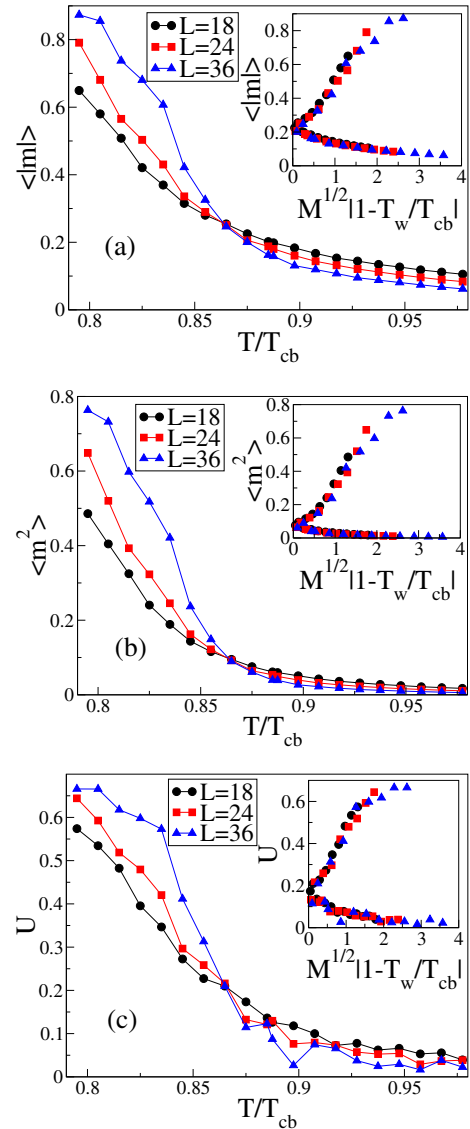


Fig. 2. Plots of (a) the average absolute value of the magnetization ($\langle |m| \rangle$), (b) the average square magnetization ($\langle m^2 \rangle$), and (c) the cumulant (U) versus the temperature relative to the bulk critical point, obtained for samples of different sizes (as indicated). Data corresponding to fields given by equation (5) with $\lambda = 16$ and $H_{\max}/J = 1.00$, so that $H_{\text{eff}} = 0.50$ (see Eq. (3)). All sample sizes have the same generalized aspect ratio $c = L^2/M = 9/8$. The common intersection point at $T_w/T_{cb} = 0.872 \pm 0.01$ allows us to locate the critical wetting temperature [24]. The insets in these figures show the corresponding scaling plots of the observable already shown in the main panel. Further details are given in the text.

follows from Abraham's exact solution. On the other hand, for $x = 3\lambda/4$ (with $\delta H_{\max} = 0.7227/2$) we obtained $T_w = 0.919$, again in full agreement with Abraham's exact result, namely, $T_w(H_{\max} = 0.36135) = 0.931029$. So, we conclude that the Ising strip in the presence of two fields acting along the wall, i.e., our $M \rightarrow \infty$ limit of $H_1(x, \lambda)$ given by equation (7), behaves as two almost

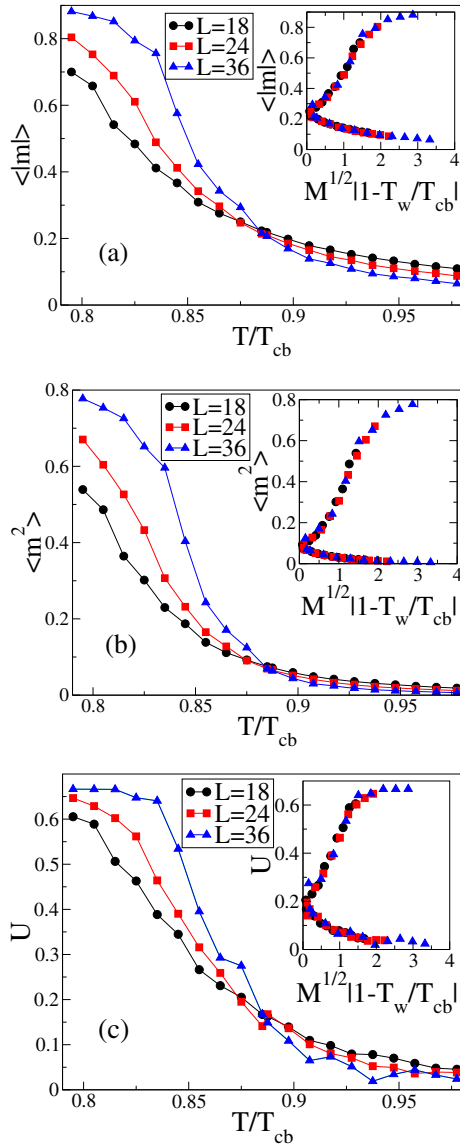


Fig. 3. Plots of (a) the average absolute value of the magnetization ($\langle |m| \rangle$), (b) the average square magnetization ($\langle m^2 \rangle$), and (c) the cumulant (U) versus the temperature relative to the bulk critical point, obtained for samples of different sizes (as indicated). Data corresponding to fields given by equation (5) with $\lambda = 32$ and $H_{\max}/J = 1.00$, so that $H_{\text{eff}} = 0.50$ (see Eq. (3)). All sample sizes have the same generalized aspect ratio $c = L^2/M = 9/8$. The common intersection point at $T_w/T_{cb} = 0.879 \pm 0.01$ allows us to locate the critical wetting temperature [24]. The insets in these figures show the corresponding scaling plots of the observable already shown in the main panel. Further details are given in the text.

independent systems, each of them having its own critical wetting temperature.

In order to illustrate this statement, Figure 6 shows a comparison of magnetization profiles obtained at (i) $T \simeq T_w(x = \lambda/4)$ and at (ii) $T \simeq T_w(x = 3\lambda/4)$. For case (i) one has that by choosing $x = \lambda/4$ the profile is almost linear as expected for the wet phase, while for $x = 3\lambda/4$ the profile corresponds to a typical nonwet state with the in-

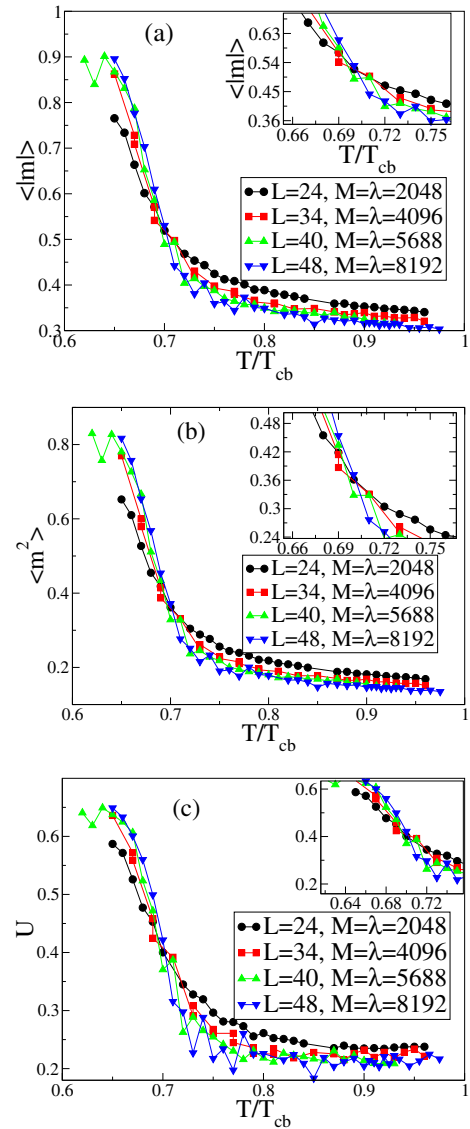


Fig. 4. Plots of (a) the average absolute value of the magnetization ($\langle |m| \rangle$), (b) the average square magnetization ($\langle m^2 \rangle$), and (c) the cumulant (U) versus the temperature relative to the bulk critical point, obtained for samples of different sizes (as indicated). Data were obtained within a wide interval centered around $x = \lambda/4$, where $H_{\max}/J = 0.7227$ (see Eq. (7)). The common intersection point at $T_w/T_{cb} = 0.699 \pm 0.01$ allows us to locate the critical wetting temperature [24]. The insets in these figures show the zoom of plots of the observable already shown in the main panel. Further details are given in the text.

terface localized close to the right-hand side of the sample. In contrast, for case (ii) the profile measured for $x = \lambda/4$ is deep in the wet phase ($T = 0.92 \gg T_{cw} = 0.699$), while the profile obtained for $x = 3\lambda/4$ is just in the wet phase. In fact, our results are also confirmed by the snapshot configurations shown in Figure 7. Figure 7a was obtained for $T/T_{cb} = 0.69 \simeq T_w/T_{cb}(x = \lambda/4)$, where one observes that the lower part of the figure (where one has $H_{\max} = 0.7227$) corresponds to a wet state with the interface highly fluctuating along the middle of the sample, while the upper part

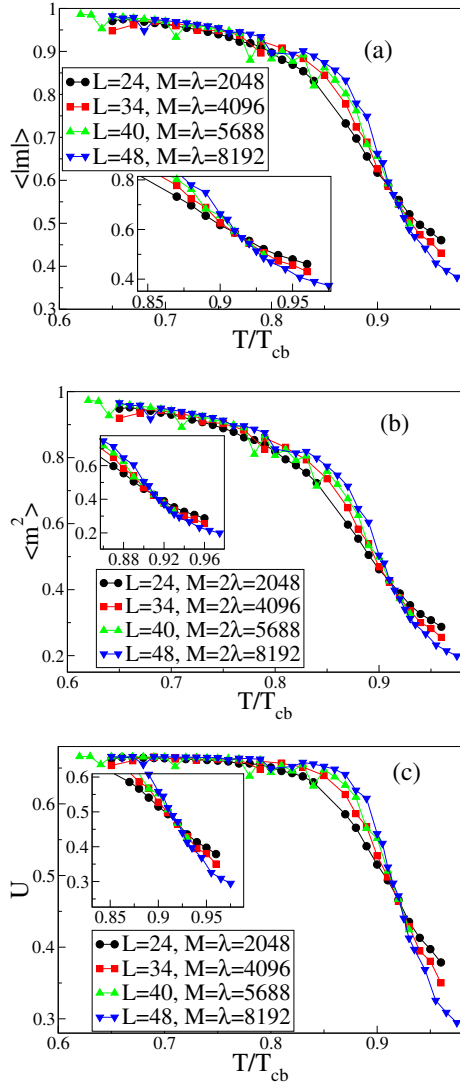


Fig. 5. Plots of (a) the average absolute value of the magnetization ($\langle |m| \rangle$), (b) the average square magnetization ($\langle m^2 \rangle$), and (c) the cumulant (U) versus the temperature relative to the bulk critical point, obtained for samples of different sizes (as indicated). Data were obtained within a wide interval centered around $x = 3\lambda/4^{-1}$, where $\delta H_{\max}/J = 0.7227/2$ ($\delta = 0.50$) (see Eq. (7)). The common intersection point at $T_w/T_{cb} = 0.919 \pm 0.01$ allows us to locate the critical wetting temperature [24]. The insets in these figures show the zoom of plots of the observable already shown in the main panel. Further details are given in the text.

of the figure (with $H_{\max} = 0.7227/2$) shows a clear nonwet phase. Figure 7b shows a zoom obtained close to the center of the sample ($x \simeq \lambda/2 \simeq M/2$) so that the abrupt change in the location of the interface can already be clearly seen. On the other hand, Figure 7c corresponds to a configuration taken at $T/T_{cb} = 0.93 \simeq T_w/T_{cb}$ ($H_{\max} = 0.36$). Here, both the upper and the lower parts of the sample are wet and the zoom of the central part of the sample ($x \approx \lambda/2 = M/2$) does not exhibit any particular feature in contrast with the case measured at $T = 0.69$ (see Fig. 7b).

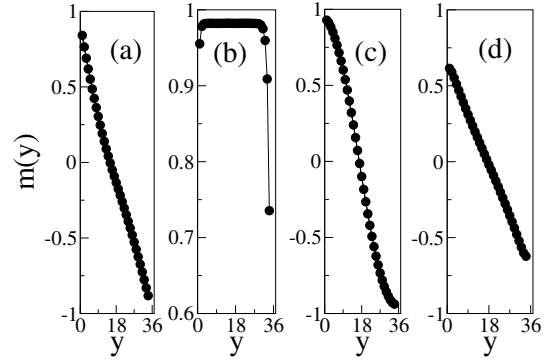


Fig. 6. Plots of the magnetization profiles $m(y)$ versus the row index y obtained for samples of size $L = 34$, $M = 4096$, and surface fields given by equation (7), with $H_{\max}/J = 0.7227$, $\delta = 0.50$ and $\lambda = M = 4096$. (a) Data measured at $x = \lambda/4^{-1}$, $T/T_{cb} = 0.69 \simeq T_w/T_{cb}$ ($H_{\max} = 0.7227$), (b) data measured at $x = 3\lambda/4^{-1}$, for $T/T_{cb} = 0.69 < T_w/T_{cb}$ ($H_{\max} = 0.7227$), (c) data measured at $x = \lambda/4$, $T/T_{cb} = 0.92 > T_w/T_{cb}$ ($H_{\max} = 0.7227$), (d) data measured at $x = 3\lambda/4$, $T/T_{cb} = 0.92 \simeq T_w/T_{cb}$ ($H_{\max} = 0.7227/2$).

Also, for the sake of completeness it is worth mentioning that for $x \simeq \lambda/2$, i.e., when the magnitude of the surface field changes abruptly, the magnetization largely fluctuates and the behavior of the system in that region cannot be well described in terms of wetting arguments (for a qualitative insight into that situation, see the middle part of the snapshot shown in Figs. 7a and 7b).

Finally, let us analyze the case of a spatially oscillatory surface field, as given by equation (6), with $\langle H_1(x) \rangle = 0 = H_{\text{eff}}$, and within the short wavelength regime (more specifically, for $\lambda = 4$), where one has that for $n\lambda + 1, n\lambda + 2, n\lambda + 3$, and $n\lambda + 4$ ($n = 0, 1, 2, \dots, M/4$) the field adopts discrete values given by $H_{\max}, 0, -H_{\max}$ and 0 , respectively. So, it is expected this “antiferromagnetic like” surface field would be unable to induce the formation of magnetic domains of different orientations with a well-defined interface running along the x direction. In this situation, the system will undergo a standard order-disorder transition in the bulk rather than a wetting transition. Now, by considering Ising strips at criticality confined between walls with free boundary conditions and a coarse grained vanishing surface field, it is known that the system shows patterns of alternating domains of different magnetization (with interfaces running perpendicularly to confinement walls) [62]. So, one has to analyze the data by means of (isotropic) finite size scaling methods, i.e., by keeping the aspect ratio $L/M = \text{constant}$, rather than by the generalizad aspect ratio $c = L^2/M = \text{constant}$ as in the case of anisotropic scaling of wetting transitions. Figures 8a and 8b show plots of $\langle |m| \rangle$ and U versus T obtained for samples of different sizes, respectively. The cumulants (Fig. 8b) exhibit a common intersection point for $T/T_{cb} = 0.99(2)$, so that we are actually in the presence of the standard (bulk) order-disorder transition of the Ising magnet. Furthermore, the data obey standard finite-size scaling, as shown in the insets of Figure 8, namely, one

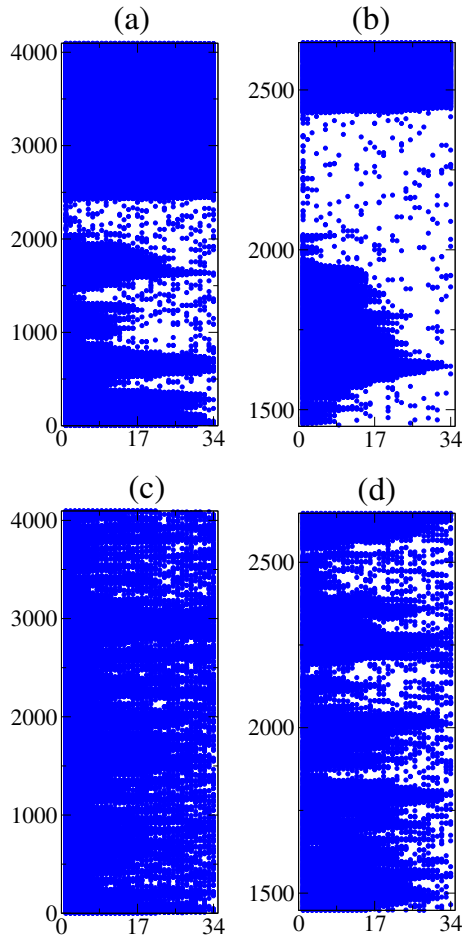


Fig. 7. Snapshot configurations obtained for lattices of size $L = 34$ and $M = \lambda = 4096$, and a bivaluated surface field given by equation (7) with $H_1/J = 0.7227$ and $\delta = 0.50$. In (a) we take $T/T_{cb} = 0.69$, while (b) shows a zoom of (a) taken close to the center of the sample $1448 \leq x \leq 2648$, (c) corresponds to $T/T_{cb} = 0.93$, while (d) shows the zoom of the central part of (c) taken for $1448 \leq x \leq 2648$. Spins pointing up are shown in blue (dark grey in the printed version) while spins pointing down are left in white.

obtains data collapse by assuming [62]

$$\langle |m| \rangle \sim L^{-\beta/\nu} \tilde{m} \left((T - T_{cb}) L^{1/\nu}, L/M \right), \quad (16)$$

and

$$U \sim \tilde{U} \left((T - T_{cb}) L^{1/\nu}, L/M \right), \quad (17)$$

where \tilde{m} and \tilde{U} are suitable scaling functions that do not need to be specified here. Also, $\beta = 1/8$ and $\nu = 1$ are the order parameter and correlation length critical exponents corresponding to the $d = 2$ Ising universality class.

It is worth mentioning that our results shown in Figure 8 are in full agreement with the experiments performed by Zdyb and Bauer [48] for the adsorption of gold on W(100) stepped surfaces. In fact, the observed order disorder transition in the adsorbed Au monolayer can be ascribed to the Ising universality class with critical exponents $\beta = 1/8$ and $\nu = 0.99 \pm 0.007$. Also, the effective

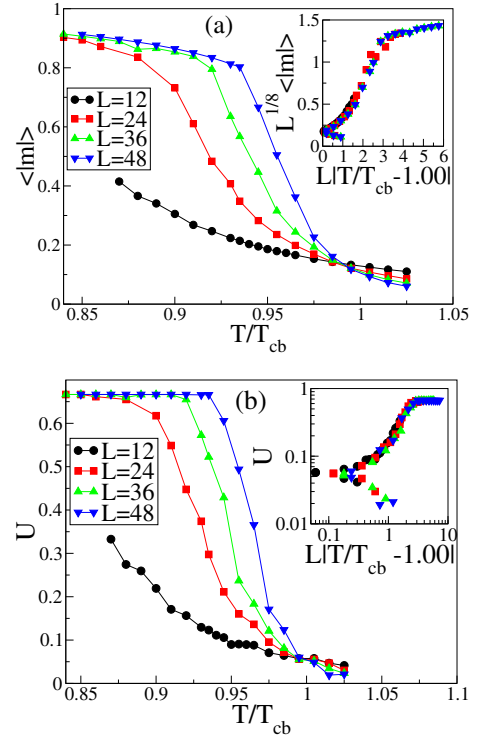


Fig. 8. Plots of (a) the average absolute value of the magnetization ($\langle |m| \rangle$) and (b) the cumulant (U) versus the temperature relative to the bulk critical point obtained for samples of different sizes (as indicated). Data corresponding to $\lambda = 4$ and $H_{\max}/J = 0.7227$, $L = 12$, $M = 256$, $L = 24$, $M = 512$, $L = 36$, $M = 768$ and $L = 48$, $M = 1024$. All sample sizes have the same aspect ratio $c = L/M = 3/128$. The intersection point of the cumulant at $T_w/T_{cb} = 0.99 \pm 0.01$ allows us to locate the critical temperature. The insets in these figures show the corresponding scaling plots of the observable already shown in the main panel. Further details are given in the text.

dependence of the exponent β on the terrace width can be explained within the framework of the theory of finite size effects, which predicts a shift of the critical temperature and the rounding of the order parameter, cf. equations (16) and (17).

6 Conclusions

Based on the exact solution of the critical wetting phase diagram developed by Abraham [30] for the case of short-range homogeneous fields acting at the walls of a confined Ising magnet, as well as on a recently proposed anisotropic finite-size scaling theory describing that situation [24,25], we addressed critical wetting behavior in the presence of inhomogeneous short-range surface fields. By assuming a spatial dependence of the fields given by $H_1(x, \lambda)$, $1 \leq x \leq M$, where M is the length of the confinement wall and λ is the spatial wavelength or period, we found that in some cases the situation can be rationalized in terms of an effective field $H_{\text{eff}} \equiv \frac{1}{\lambda} \int_0^\lambda H_1(x, \lambda) dx$ (where $M = n\lambda$, so H_{eff} is a coarse-grained surface field up to

a certain wavelength or spatial period λ). For example, if $H_{\text{eff}} > 0$, and in the short wavelength regime (we actually numerically explored the case for $\lambda \leq 1.28$, i.e., $\lambda < M$, and $\lambda \ll \zeta_{\parallel} \rightarrow \infty$), the wetting transition is well described taking $H_{\text{eff}} \equiv F(T)$, where $F(T)$ is the exact solution worked out by Abraham [30] given by equation (1). The long wavelength regime is studied by taking a bivaluated surface field (H_{max} for $x \leq \lambda/2$; δH_{max} for $x > \lambda/2$, with $\lambda = M$ and $0 < \delta \leq 1$). In this case, the regions of the strip located far away from the middle behave almost independently exhibiting their own critical wetting temperatures, which are in full agreement with those temperatures predicted by equation (1) for the respective surface fields (namely H_{max} and δH_{max}). On the other hand, for a rapidly varying field of small wavelength such that $H_{\text{eff}} = 0$ (specifically for a sinusoidal field with $\lambda = 4$) we no longer observe wetting transitions but a standard bulk order-disorder transition at T_{cb} . This case turns out to be equivalent to considering a strip in the absence of boundary fields since bulk criticality is approached by the onset of an alternating structure of magnetic domains of different orientations with interfaces running in the direction perpendicular to the confining walls.

Summing up, we expect that our study will contribute to understanding interfacial phenomena in systems confined between inhomogeneous walls.

This work was supported by CONICET through PIP 143 and the Universidad Nacional de La Plata, Argentina.

References

- J.S. Rowlinson, B. Widom, *Molecular Theory of Capillarity* (Oxford University Press, Oxford, 1982)
- D.E. Sullivan, M.M. Telo da Gama, in *Fluid Interfacial Phenomena*, edited by C. Croxton (Wiley, New York, 1986), p. 45
- S. Dietrich, in *Phase Transitions and Critical Phenomena*, edited by C. Domb, J.L. Lebowitz (Academic, London, 1988), Vol. 12, p. 1
- M. Schick, in *Liquids at Interfaces*, edited by J. Charvolin, J.-F. Joanny, J. Zinn-Justin (Elsevier, Amsterdam, 1990), p. 415
- D. Bonn, D. Ross, Rep. Progr. Phys. **64**, 1085 (2001)
- P.G. De Gennes, F. Brochard-Wyart, D. Quéré, *Capillarity and Wetting Phenomena: Drops, Bubbles, Pearls, Waves* (Springer, Berlin, 2003)
- M. Schön, S. Klapp, *Nanoconfined Fluids: Soft Matter Between Two and Three Dimensions* (J. Wiley & Sons, New York, 2006)
- Low and High Temperature Wetting: State of the Art*, Ann. Revs. Mater. Res., edited by D.R. Clarke, M. Rühle, A.P. Tomsia (Ann. Revs., Palo Alto, 2008), Vol. 38
- D. Bonn, J. Eggers, J.O. Indekeu, J. Meunier, E. Rolley, Rev. Mod. Phys. **81**, 739 (2009)
- Multilayer Thin Films: Sequential Assembly of Nanocomposite Materials*, edited by G. Decker, J.B. Schlenoff (Wiley-VCH, Weinheim, 2002)
- Nano-Architected and Nano-Structured Materials*, edited by Y. Champion, H.-J. Fecht (Wiley-VCH, Weinheim, 2004)
- Handbook of Nanostructured Thin Films and Coatings*, edited by S. Zhang (CRC Press, Boca Raton, 2010), Vols. 1–3
- S. Dietrich, M.N. Popescu, M. Rauscher, J. Phys.: Condens. Matter **17**, 577 (2005)
- D. Quéré, Rep. Prog. Phys. **68**, 2495 (2005)
- C. Borgs, J. De Coninck, R. Kotecky, M. Zinque, Phys. Rev. Lett. **74**, 2292 (1995)
- P. Swain, R. Lipowsky, Langmuir **14**, 6772 (1998)
- J. De Coninck, J. Ruiz, S. Miracle-Sole, Phys. Rev. E **65**, 036139 (2002)
- K. Grabowski, A. Patrykiewicz, S. Sokolowsky, E.V. Albano, A. de Virgiliis, Surf. Sci. **448**, 11 (2000)
- P.R. Pandey, S. Roy, J. Phys. Chem. Lett. **4**, 3692 (2013)
- B. Zhang, J. Wang, X. Zhang, Langmuir **29**, 6652 (2013)
- M. Trobo, E.V. Albano, Phys. Rev. E **88**, 052407 (2013)
- K. Binder, D.P. Landau, M. Müller, J. Stat. Phys. **110**, 1411 (2003)
- E.V. Albano, K. Binder, D.W. Heermann, W. Paul, Surf. Sci. **223**, 151 (1989)
- E.V. Albano, K. Binder, Phys. Rev. E **85**, 061601 (2012)
- E.V. Albano, K. Binder, Phys. Rev. Lett. **109**, 036101 (2012)
- E.V. Albano, K. Binder, W. Paul, J. Phys.: Condens. Matter **12**, 2701 (2000)
- F. Parisen Toldin, M. Tröndle, S. Dietrich, Phys. Rev. E **88**, 052110 (2013)
- F. Parisen Toldin, S. Dietrich, J. Stat. Mech. **2010**, P11003 (2010)
- N.G. Fytas, W. Selke, Eur. Phys. J. B **86**, 365 (2013)
- D.B. Abraham, Phys. Rev. Lett. **44**, 1165 (1980)
- L.W. Bruch, R.D. Diehl, J.A. Venables, Rev. Mod. Phys. **79**, 1381 (2007)
- H.-J. Elmers, Int. J. Mod. Phys. B **9**, 3115 (1995)
- J. Bandlow, P. Kaghazchi, T. Jacob, C. Papp, B. Tränkenschuh, R. Streber, M.P.A. Lorenz, T. Fuhrmann, R. Denecke, H.-P. Steinrück Phys. Rev. B **83**, 174107 (2011)
- P. Zeppenfeld, S. Horch, G. Comsa, Phys. Rev. Lett. **73**, 1259 (1994)
- S. Horch, P. Zeppenfeld, G. Comsa, Appl. Phys. A **60**, 147 (1995)
- M. Dienwiebel, P. Zeppenfeld, J. Einfeld, G. Comsa, F. Picaud, C. Ramseyer, C. Girardet, Surf. Sci. **446**, L113 (2000)
- H. Hövel, B. Grimm, B. Reihl, Surf. Sci. **477**, 43 (2001)
- J.-Y. Park, S.-J. Kahng, U.D. Ham, Y. Kuk, K. Miyake, K. Hata, H. Shigekawa, Phys. Rev. B **60**, 16934 (1999)
- P.W. Davis, M.A. Quinlan, G. Somorjai, Surf. Sci. **121**, 290 (1982)
- V. Marsico, M. Blanc, K. Kuhnke, K. Kern, Phys. Rev. Lett. **78**, 94 (1997)
- V. Pouthier, C. Ramseyer, C. Girardet, K. Kuhnke, V. Marsico, M. Blanc, R. Schuster, K. Kern, Phys. Rev. B **56**, 4211 (1997)
- W. Widdra, P. Trischberger, W. Friess, D. Menzel, S.H. Payne, H.J. Kreuzer, Phys. Rev. B **57**, 4111 (1998)
- F. Picaud, V. Pouthier, C. Ramseyer, C. Girardet, Surf. Rev. Lett. **6**, 669 (1999)
- M. Wagner, F.R. Negreiros, L. Sementa, G. Barcaro, S. Surnev, A. Fortunelli, F.P. Netzer, Phys. Rev. Lett. **110**, 216101 (2013)

45. J.J. Zhang, G. Katsaros, F. Montalenti, D. Scopece, R.O. Rezaev, C. Mickel, B. Rellinghaus, L. Miglio, S. De Franceschi, A. Rastelli, O.G. Schmidt Phys. Rev. Lett. **109**, 085502 (2012)
46. J. Guo, Y. Mo, E. Kaxiras, Z. Zhang, H.H. Weitering, Phys. Rev. B **73**, 193405 (2006)
47. N.N. Negulyaev, V.S. Stepanyuk, W. Hergert, P. Bruno, J. Kirschner, Phys. Rev. B **77**, 085430 (2008)
48. R. Zdyb, E. Bauer, Phys. Rev. Lett. **100**, 155704 (2008)
49. S.R. Lu, R. Yu, J. Zhu, Phys. Rev. B **87**, 165436 (2013)
50. M. Krawiec, M. Jaochowski, Phys. Rev. B **82**, 195443 (2010)
51. L. Li, L. Luo, J. Ciston, W.A. Saidi, E.A. Stach, J.C. Yang, G. Zhou1, Phys. Rev. Lett. **113**, 136104 (2014)
52. M. Godoy, A.J. Moreno, G.A. Jorge, H.J. Ferrari, P.S. Antonel, J.L. Mietta, M. Ruiz, R.M. Negri, M.J. Pettinari, V. Bekeris, J. Appl. Phys. **111**, 044905 (2012)
53. E.V. Albano, K. Binder. J. Stat. Phys. **157**, 436 (2014)
54. A. Maciolek, J. Stecki, Phys. Rev. B **54**, 1128 (1996)
55. P. Nowakowski, M. Napiórkowski, Phys. Rev. E **78**, 060602(R) (2008)
56. L. Onsager, Phys. Rev. **65**, 117 (1944)
57. K. Binder, J.S. Wang, J. Stat. Phys. **55**, 87 (1989)
58. K. Binder, in *Finite Size Scaling and Numerical Simulation of Statistical Systems*, edited by V. Privman (World Scientific, Singapore, 1990), p. 173
59. K. Binder, Phys. Rev. Lett. **47**, 693 (1981)
60. K. Binder, Rep. Prog. Phys. **60**, 487 (1997)
61. O. Dillmann, W. Janke, M. Müller, K. Binder, J. Chem. Phys. **114**, 5823 (2001)
62. E.V. Albano, K. Binder, Dieter W. Heermann, W. Paul, Z. Phys. B **77**, 445 (1989)